Biochimica et Biophysica Acta 1817 (2012) 658–665

Contents lists available at SciVerse ScienceDirect

Biochimica et Biophysica Acta

journal homepage: www.elsevier.com/locate/bbabio

Structural changes that occur upon photolysis of the $Fe(II)_{a3}$–CO complex in the cytochrome ba_3-oxidase of *Thermus thermophilus*: A combined X-ray crystallographic and infrared spectral study demonstrates CO binding to Cu_B ☆

Bin Liu [a,1], Yang Zhang [b], J. Timothy Sage [b,*], S. Michael Soltis [c,**], Tzanko Doukov [c], Ying Chen [a], C. David Stout [a,***], James A. Fee [a,****]

[a] The Scripps Research Institute, Department of Molecular Biology, MB-8, 10550 North Torrey Pines Road, La Jolla, CA 92037, USA
[b] Department of Physics and Center for Interdisciplinary Research on Complex Systems, Northeastern University, 110 Forsyth St., Boston, MA 02115, USA
[c] Stanford Synchrotron Radiation Lightsource, 2575 Sand Hill Road, Menlo Park, CA 94025, USA

ARTICLE INFO

Article history:
Received 14 July 2011
Received in revised form 9 December 2011
Accepted 9 December 2011
Available online 27 December 2011

Keywords:
Cytochrome c oxidase
Cytochrome ba_3 oxidase
Carbon monoxide
CO photodissociation
Thermus thermophilus
Fourier transform infrared

ABSTRACT

The purpose of the work was to provide a crystallographic demonstration of the venerable idea that CO photolyzed from ferrous heme-a_3 moves to the nearby cuprous ion in the cytochrome *c* oxidases. Crystal structures of CO-bound cytochrome ba_3-oxidase from *Thermus thermophilus*, determined at ~2.8–3.2 Å resolution, reveal a Fe–C distance of ~2.0 Å, a Cu–O distance of 2.4 Å and a Fe–C–O angle of ~126°. Upon photodissociation at 100 K, X-ray structures indicate loss of Fe_{a3}–CO and appearance of Cu_B–CO having a Cu–C distance of ~1.9 Å and an O–Fe distance of ~2.3 Å. Absolute FTIR spectra recorded from single crystals of reduced ba_3–CO that had not been exposed to X-ray radiation, showed several peaks around 1975 cm^{-1}; after photolysis at 100 K, the absolute FTIR spectra also showed a significant peak at 2050 cm^{-1}. Analysis of the 'light' *minus* 'dark' difference spectra showed four very sharp CO stretching bands at 1970 cm^{-1}, 1977 cm^{-1}, 1981 cm^{-1}, and 1985 cm^{-1}, previously assigned to the Fe_{a3}–CO complex, and a significantly broader CO stretching band centered at ~2050 cm^{-1}, previously assigned to the CO stretching frequency of Cu_B bound CO. As expected for light propagating along the tetragonal axis of the $P4_32_12$ space group, the single crystal spectra exhibit negligible dichroism. Absolute FTIR spectrometry of a CO-laden ba_3 crystal, exposed to an amount of X-ray radiation required to obtain structural data sets before FTIR characterization, showed a significant signal due to photogenerated CO_2 at 2337 cm^{-1} and one from traces of CO at 2133 cm^{-1}; while bands associated with CO bound to either Fe_{a3} or to Cu_B in "light" *minus* "dark" FTIR difference spectra shifted and broadened in response to X-ray exposure. In spite of considerable radiation damage to the crystals, both X-ray analysis at 2.8 and 3.2 Å and FTIR spectra support the long-held position that photolysis of Fe_{a3}–CO in cytochrome *c* oxidases leads to significant trapping of the CO on the Cu_B atom; Fe_{a3} and Cu_B ligation, at the resolutions reported here, are otherwise unaltered. This article is part of a Special Issue entitled: Respiratory Oxidases.

1. Introduction

1.1. Cytochrome ba_3

Cytochrome ba_3 first described in 1988 by Zimmermann et al. [1] and characterized in detail by Keightley et al. [2], is now considered a B-type cytochrome *c* oxidase [3], and is one of two terminal heme–copper oxidases [4] in the Gram-negative eubacterium *Thermus thermophilus*, which couple the reduction of dioxygen to proton translocation across the inner bacterial membrane. The enzyme contains a homo-dinuclear copper center, Cu_A, a low-spin heme-*b*, and a binuclear center including a high spin heme-a_3 in close proximity to the three-coordinate Cu_B atom [1,5–7]. This binuclear center serves as the site where dioxygen is reduced to H_2O (see Ref. [8]). While time-resolved structural studies of metal bound oxygen forms of the enzyme may be the most desirable way to understand the molecular mechanism of the catalytic reaction, the diffusion limited rate of dioxygen binding [9,10] followed by its rapid reduction by the binuclear site, recommends the use of generally redox inactive carbon monoxide (CO) as an alternative to study ligand binding and coordination changes at the binuclear site, free of the complications resulting from dioxygen reduction chemistry. By exploiting the 100% quantum yield for photodissociation of heme–CO complexes [11], CO has been used to probe both Fe

Abbreviations: FTIR, Fourier transform infrared; MGy, 1×10^6 Gray; FWHM, full width at half maximum.

☆ This article is part of a Special Issue entitled: Respiratory Oxidases.

* Corresponding author. Tel.: +1 617 373 2908; fax: +1 617 373 2943.
** Corresponding author. Tel.: +1 650 926 3050; fax: +1 650 926 3600.
*** Corresponding author. Tel.: +1 858 8738; fax: +1 858 784 2857.
**** Corresponding author. Tel.: +1 858 784 9235; fax: +1 858 784 2857.
E-mail addresses: jtsage@neu.edu (J.T. Sage), soltis@slac.stanford.edu (S.M. Soltis), dave@scripps.edu (C.D. Stout), jafee@scripps.edu (J.A. Fee).
[1] Present address: Howard Hughes Medical Institute, Department of Molecular Biophysics and Biochemistry, Yale University, New Haven, CT 06520, USA.

0005-2728/$ – see front matter © 2011 Elsevier B.V. All rights reserved.
doi:10.1016/j.bbabio.2011.12.010

and Cu in the catalytic site of heme–Cu oxidases [12,13]. Indeed, CO photodissociation is a powerful tool for studying dynamic features of the active site and how it adjusts to "photo freed" CO [13–15].

The purpose of this work was to provide a crystallographic demonstration of the long-held assertion that CO bound to heme-a_3 of the cytochrome *c* oxidases moves, upon illumination, from Fe_{a3}(II) to Cu_B(I). This assignment was originally evidenced by shifts of the IR spectral line associated with the CO stretch from ~1975 cm^{-1}, arising from the CO-stretch mode of Fe-bound CO, to ~2050 cm^{-1}, thought to arise from the CO-stretch of Cu_B-bound CO [14,16,17] as suggested in Scheme 1. Recent work by Varotsis and co-workers [18] indicates, however, that the stretching frequency of non-metal bound CO may show similar values for CO bound in polar protein cavities. If proven to occur in the cytochrome *c* oxidases, such a finding would complicate the now venerable interpretation that the observed ~2050 cm^{-1} band represents the CO stretching frequency of the Cu_B–CO complex.

The heme–CO complex exhibits unusual vibrational properties in comparison with other heme proteins. The deviation of the C–O and Fe–CO frequencies from the linear correlation established for other histidine-ligated heme proteins has been attributed to compression of the C – O bond or distortion of the FeCO unit from the nearly linear geometry observed for other heme proteins [19]. The linewidths of the C–O stretching band are also unusually narrow for heme–Cu oxidases [12,13]. The frequency and oscillator strength of the photolyzed C–O have values intermediate between those of heme–CO and CO gas but are similar to those observed for CO binding to Cu proteins [20]. The high barrier for geminate rebinding of photolyzed CO to the heme (40–60 kJ/mol) in comparison with typical heme proteins (10 kJ/mol) has also been associated with the presence of Cu [12,13]. In this work, X-ray crystallography provides evidence for photo induced transfer of CO from Fe_{a3}–CO to Cu_B–CO with no other changes in metal ligation, while infrared spectroscopy shows that CO binding within a single crystal of ba_3 is highly similar to that which occurs in solution. Parallel characterization of the structure and vibrational properties of the Cu–CO complex in a heme–Cu oxidase, as presented here, serves as a springboard for structurally calibrated spectroscopic investigations.

2. Materials and methods

2.1. Protein expression, purification, and crystallization

Recombinant wild type and mutant (II-E4Q/I-K258R) cytochrome ba_3 oxidase genes were expressed in *T. thermophilus* HB8, and the enzyme was purified as described [21,22]. (Numerous observations in the Fee laboratory indicate these mutations are benign, and the results reported here support this conclusion.) Final protein samples were dissolved in 10 mM Bis–Tris pH 7.0 with 0.1 M KCl and 13 mM n-nonyl-β-D-glucopyranoside (2 times its critical micelle concentration) after performing the detergent exchange using a small DEAE resin (GE Science) in an Econo-Column (BioRad), the sample was concentrated to ~20 mg/mL using an Ultra YM-10 concentrator (Microcon). Spectral characterization was determined using an SLM/AMINCO model DB3500 dual beam spectrophotometer. The purity index, A_{413}/A_{280}, of the enzyme used in this work ranged from ≥0.7 to 0.9. Optical spectra are shown in Fig. S1. The concentration of fully constituted protein was obtained using $\Delta\varepsilon^{red}_{560-590} = 26\ mM^{-1}\ cm^{-1}$ from a reduced *minus* oxidized difference spectrum using Na-dithionite as the reductant. The protein was crystallized in air at room temperature as described (Ref. [22]); trays containing crystals so prepared were transferred into a glove box (COY Laboratory Products Inc, USA) filled with a gas mixture of 10% (v/v) hydrogen and 90% (v/v) nitrogen.

2.2. Carbon monoxide binding to ba_3 in crystals and in solution

In order to realize the CO bound state, a cryo-protectant solution [50% (±)-2-methyl-2,4-pentanediol, 14% Polyethylene Glycol 2000, 0.1 M KCl, 13 mM n-nonyl-β-D-glucopyranoside in 0.1 M Bis–Tris (pH 7.0), and 0.1 mM methyl viologen] was sparged vigorously with carbon monoxide in a fume hood for 5–10 min, sealed with Parafilm, and moved into the glove box. Several small vials containing weighed amounts of dry Na dithionite were also brought into the anaerobic chamber. After the increased O_2-levels within the chamber, caused by these operations, had returned to <1 ppm, crystals were reduced in their crystallization droplet by adding several microliters of CO saturated cryoprotectant being 10 mM in Na dithionite, and 0.1 mM methyl viologen. Droplets containing crystals were re-covered and allowed to stand for 1 to 2 min before a crystal was loaded onto a nylon loop and flash frozen in liquid nitrogen. Total time of this operation starting with reduction of the crystals was approximately 2 to 5 min. The intense blue color of the methylviologen free radical, visible in the droplet, provided continuous evidence that the droplet was reducing and oxygen free, thereby making possible the binding of CO to the Fe^{2+} form of the high-spin heme [13]. At this point in the experiment, the only assay available for Fe_{a3}–CO formation in the frozen crystal is X-ray structural determination.

2.3. X-ray data-collection, structure determination and refinement

Data sets were collected at 100 K using beam line 11-1 at the Stanford Synchrotron Radiation Lightsource at 0.979 Å and using a MAR325 detector (plus other beam lines as indicated in Table 1). Diffraction image data were processed with the programs MOSFLM [23] and SCALA [24]. The wild type recombinant structure, (PDB ID: 1XME) was utilized as the initial model to obtain phase information using molecular replacement with PHASER [25].

Initially, the structures were refined by rigid body refinement followed by restrained refinement with REFMAC 5.0 [26]. Without including carbon monoxide in the refinements, the $|F_o–F_c|$ electron density maps clearly indicated the likely presence of a CO molecule between Fe_{a3}- and Cu_B that was best modeled by a CO molecule bound to the Fe_{a3} or Cu_B and in a configuration somewhat off perpendicular to the plane of heme-a_3. CO was further treated as a free molecule having a bond length of 1.128 Å in subsequent refinements with an allowed deviation of ±0.005 Å. A better fit to the $|F_o–F_c|$ map was always obtained when the C-atom was involved in bonding to either to Fe or Cu. COOT [27] was utilized to display structure models and electron density maps. Details of data collection statistics and final refinement statistics are given in Table 1. Structural figures were created

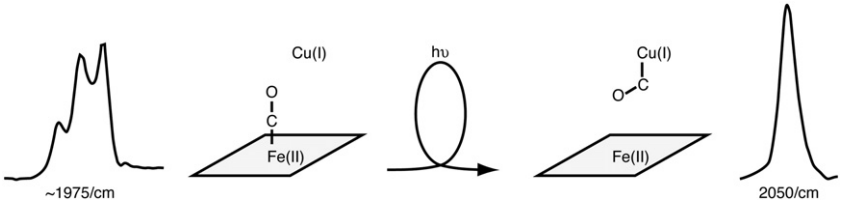

Scheme 1. Scheme depicting protoinduced CO transfer from Fe(II)-CO to form Cu(I)-CO. Typical difference spectra are also shown.

Table 1
Data collection and refinement statistics.

Data set	[a]WT (A2)	[a]WT (A2_2)	[b] Mutant (J2)	Mutant [b](L1)	W.T. [a] (C1)	W.T. [a] (E7)
[c]Timing of X-ray	Before	After	Before	Before	After	After
[g]Absorbed dose (MGy)	11.1	20.8	20.3	10.6	10.8	9.39
SSRL Beam line	11-1	9-2	11-1	11-1	11-1	7-1
Flux@200 mA (p/s)	5.67×10^{11}	5.03×10^{11}	3.9×10^{11}	3.9×10^{11}	4.71×10^{11}	2.64×10^{11}
[d]Resolution (Å)	2.90 (3.06–2.90)	3.20 (3.37–3.20)	2.80 (2.87–2.80)	2.95 (3.11–2.95)	2.90 (3.06–2.90)	2.80 (2.95–2.80)
Space group	$P4_32_12$	$P4_32_12$	$P4_12_12$	$P4_12_12$	$P4_32_12$	$P4_32_12$
$a=b$, c (Å)	108.77, 164.60	108.81, 164.46	114.21, 146.93	114.96, 148.56	109.75, 164.77	109.96, 168.72
Total observations	74,069	87,276	140,705	57,127	135,443	145,901
Unique reflection	22,594	16,200	24,625	19,662	22,314	24,669
[d]Redundancy	3.3 (3.2)	5.4 (6.9)	5.7 (7.2)	2.9 (2.9)	6.1 (6.3)	5.9 (4.9)
[d]Completeness (%)	99.9 (100)	96.6 (97.6)	100 (100)	92.1 (92.1)	97.6 (97.6)	94.9 (94.9)
[d]$<I/\sigma_I>$	14.4 (4.1)	5.2 (2.0)	11.1 (1.7)	3.5 (1.8)	3.9 (2.0)	3.8 (2.1)
[d,e]R_{sym} (%)	2.1 (17.8)	6.0 (38.5)	4.6 (44.3)	7.4 (38.3)	10.8 (35.7)	11.1 (35.6)
R.m.s. deviations						
Bond lengths (Å)	0.014	0.011	0.017	0.015	0.015	0.017
Bond angles (°)	1.731	1.488	2.086	2.022	1.761	1.807
R_{work}/R_{free} (%)	22.9/28.4	31.8/36.7	21.5/26.5	25.8/32.3	28.6/32.9	21.9/27.4
[f]PDB ID	3QJQ	3QJR	3QJS	3QJT	3QJU	3QJV

[a] WT refers to recombinant wild-type enzyme.
[b] Mutant here refers to the II-E4Q/I-K258R double mutation.
[c] Timing with respect to photolysis.
[d] Values in parentheses are for the last shell.
[e] $R_{sym}=\sum |I-\langle I\rangle|/\sum I$, where I is the integrated intensity for a reflection for all symmetry equivalent reflections.
[f] World wide protein data bank codes.
[g] Computed using RADDOSE [29].

using PyMOL [28]. Absorbed doses of X-ray radiation were calculated using RADDOSE [29].

2.4. Photodissociation of crystalline and solution ba_3–CO

Photodissociation of CO from heme-a_3 was accomplished at 100 K by mounting a crystal in the cryostream around which were disposed the two objectives of a microspectrophotometer necessary to focus light from a Hg/Xe or a deuterium/halogen lamp onto the crystal. The optical absorption spectrum of the crystal was repeatedly recorded until there were no further changes; this operation was usually complete in a few minutes. See Fig. S2 for an example of such a spectrum, and see Ref. [30] and references therein for additional detail. Currently, single crystal spectrophotometers are available at both TSRI and SSRL (see Liu et al. [30]).

Infrared measurements on a frozen ba_3–CO solution under identical conditions provide a comparison for the crystal measurements. A ~3 mM solution of ba_3 in a sealed tube was purged with argon to eliminate oxygen. This resulted in a further concentration of the enzyme, which was then equilibrated for several minutes under 1 atm CO, and reduced with a small excess of sodium dithionite, introduced as a concentrated solution in Tris buffer, pH 7.5. A gastight syringe was then used to transfer a small drop of the enzyme solution onto an empty cryoloop that was mounted on the microscope stage. Thereafter, a dry pipette tip was used to remove excess solution from the loop, after which it was moved into the cryostream.

2.5. Preparation for and recording of single crystal FTIR spectra

A commercially available infrared microscope (Bio-Rad UMA-500) was modified at Northeastern University to allow magnetic mounting and positioning of cryoloops containing individual crystals, and to introduce visible laser illumination into the optical train. The long working distance of the Schwarzschild microscope objective provides access for the nozzle of a cryocooler (Oxford Cryosystems 700 Series) that is used to maintain the temperature of a crystal mounted at its focus at temperatures as low as 100 K. Crystals were transferred under liquid nitrogen from a storage dewar to a magnet on the goniometer head affixed to the microscope stage.

Exposure to the microscope illuminator during mounting and alignment leads to complete photolysis of the crystal. Prior to light–dark measurements, the crystal was annealed by repeated manual blocking of the cryostream for 2–10 s intervals, until no changes were seen in the 2050 cm^{-1} absorption feature in the single-beam FTIR spectrum. Light–dark absorbance changes were then determined by subtraction of spectra recorded before and after illumination.[2]

All infrared measurements were performed at 2 cm^{-1} resolution at 100 K, using a Bio-Rad FTS-40A interferometer. To avoid photolysis of CO observed over periods of tens of minutes under exposure to ambient light, all measurements were performed in the dark. A long wave pass optical filter with a 2500 cm^{-1} cutoff frequency, placed in the IR beam prior to the sample, prevented photolysis by the 632.8 nm FTIR alignment laser. Triangular apodization was employed for Fourier transformation. The absolute infrared absorbance of the crystals was calculated with reference to the spectrum of the unobstructed IR beam. Infrared difference spectra of crystals and solutions were corrected by subtraction of water vapor and of a polynomial baseline.

3. Results and discussion

The cytochrome ba_3-oxidase from *Tt* is a good system with which to obtain *in crystallo*, both spectral and X-ray diffraction evidence for the positions of CO binding in "dark" prepared crystals, in which there is no question that CO is bound to Fe_{a3}, and in "light" prepared crystals to reveal the structural consequences of the photochemical liberation of CO. The strategies used were as follows. Ideally, one would like to bind CO in the dark, obtain a low temperature X-ray structure

[2] Detailed kinetics measurements showed that either 1450 s illumination with 10 μW of the 441.6 nm line from a helium cadmium laser beam focused to a 150 μm diameter or 800 s illumination with approximately 10 μW of light from the microscope illuminator, focused to an 800 μm diameter, induced complete CO photolysis with identical spectral changes. Note that the infrared beam itself does not induce photolysis.

along with optical and IR spectra from the same crystal, subsequently expose the crystal to visible light to liberate CO, and obtain an X-ray structure along with optical and IR spectra — all from the same crystal. Unfortunately, such a scheme will not work. The first problem arises from the necessity to align the crystal in a position that allows obtaining both optical and IR spectra. In order to visualize the crystal, this method of alignment requires placement of the crystal in the tightly-focused beam of a micro-spectrophotometer. Experience shows that even the imperceptibly weak lamp intensities used during this process photolyze the Fe_{a3} – CO bond. At 100 K this is effectively irreversible [31]. Once it is properly located in the optical/IR beam, however, the crystal containing "photo-freed" CO can be annealed (by repeated raising and lowering of the temperature), such that the CO returns quantitatively to ferrous Fe_{a3} and the same "light"–"dark" difference spectra are obtained even after repeated cycling. Unfortunately, this leads to a second problem, namely that annealing a crystal of ba_3 in this manner, even for a few seconds, generally leads to a debilitating loss of high angle diffraction such that information on the position of CO in either "dark" or "light" forms is lost. To negotiate these obstacles and still capture diffraction, optical, and IR data, we carried out the following experiments.

3.1. Results from X-ray diffraction

Referring to Table 1, crystal A2 was converted to its "dark," carbonylated form in La Jolla and shipped under liquid nitrogen to SSRL for X-ray structure determination. (Light levels in the experimental enclosure were weak enough to avoid CO photolysis during data collection.) The approximate total time of X-ray exposure was ~3500 s with indicated doses in MGy shown in Table 1. The results of analyzing the A2 data set are given in column 2 of Table 1. These data revealed the association of CO with Fe_{a3}, as shown in Fig. 1a. The same crystal, renamed as A2_2, was then photolyzed at 100 K in the beam of the micro spectrophotometer at SSRL in the course of obtaining its visible optical absorption spectrum. Fig. S2 reveals that both heme-*b* and heme-a_3 are substantially, if not fully, reduced during the course of this experiment, as seen previously [30].[3] Crystal A2_2 was then subjected to another round of X-ray data collection, adding an additional 9.7 MGy dose to give a total dose of 20.8 MGy. Its crystallographic properties are listed in column 3 of Table 1. Fig. 1b shows the CO omit map that provides evidence for the presence of CO between the Fe_{a3} and Cu_B atoms in the "light," carbonylated A2_2 crystal. After recording the diffraction data for the latter, crystal A2_2 was shipped under liquid nitrogen to Boston for recording absolute IR and "light"–"dark" difference FTIR spectra (see below). Fig. 1c shows the CO omit maps in a different perspective. That labeled A2 corresponds to the Fe-bound, "dark" ba_3–CO structure while that labeled A2_2 shows an omit map for the Cu_B-bound, "light" ba_3–CO structure.

Five additional crystals were examined. Crystal A3 (not described in Table 1) diffracted only to ~3.7 Å, and was examined by FTIR spectrometry only after exposure to a dose of 18.4 MGy of X-ray radiation (see below). In addition, two crystals containing the double crystal mutation ($P4_12_12$, Table 1) were examined prior to or after exposure to X-ray radiation (Table 1). The metrics of the three Fe_{a3}–CO, "dark," structures, presented in Table 1, are shown in Table 2: WT crystal A2, mutant crystal (J2), and mutant crystal (L1). The average Fe–C distance is ~1.95 ± 0.04 Å while the average Cu_B–O distance is ~2.42 ± 0.11 Å, distances that indicate coordinate covalent Fe – CO bonding in the "dark" structures and very weak if any such bonding between the O-atom of CO and Cu_B in these structures. The average Fe – C – O bond angle is ~126 ± 8°, suggesting repulsion between the O-atom of the Fe-bound CO and Cu_B, causing this apparent shift of ~54° from a heme–Fe–CO angle of 180°. These metrics are quite similar to those reported for the fully reduced, carbonylated form of bovine aa_3-oxidase [32]: Fe–C, 1.90; Cu–O, 2.4 Å, and Fe–C–O, 152°.

The metrics of three "photo-freed," "light," or "after" structures are also given in Table 2: WT crystals A2_2, C1, and E7. Under the working assumption that it is the C-atom of CO that binds to Cu_B, the average Cu_B–C distance is ~1.92 ± 0.03 Å and the average Fe_{a3}–O distance is 2.70 ± 0.49 Å (Table 2) indicating coordination of the C-atom of CO to Cu_B and the absence of, or very weak, interaction of the O-atom of CO to the Fe-atom in the "light" structures. The average Cu_B–C–O angle is 129 ± 20° while the average Fe–C–O angle is 126 ± 8° indicating that the geometry of the CO in the two structures differs by an approximate 180° flip with minor translation to accommodate the different bonding situations in the Fe – CO *vs.* the Cu – CO structures (see Figs. 1c and S3). Notably, in the bovine oxidase, Muramoto et al. [33] report what may be a side-on arrangement of the C- and O-atoms when bound to Cu_B: Cu–O, 2.7 Å; and Cu–C, 2.4 Å. However, because these distances are nominally outside the expected bonding envelope, these data suggest a more complicated arrangement between the metals and CO in the 100 K structure of bovine oxidase.

3.2. Infrared spectroscopy of single crystals

Exposure to visible light during optical alignment in the IR microscope photolyzes ba_3–CO crystals, as reflected by a feature near 2050 cm^{-1} in the absolute spectra shown in Fig. 2. For crystal b4, which had not been exposed to X-ray radiation, no changes in the area of this line were observed after more than 24 h, thus confirming that photolysis is complete and irreversible at 100 K and that other photolytic events do not appear to be occurring. Upon annealing the crystal in the dark, however, the intensity of this feature decreases, accompanied by the appearance of features near 1975 cm^{-1} associated with Fe_{a3}–CO. After the feature decreased to 23% of its original area, as shown in the upper spectrum, no changes were apparent on further annealing.

Fig. 3 (upper portion) compares light–dark absorbance differences recorded in the C–O stretching region upon illumination of annealed cytochrome ba_3–CO solutions and crystals at 100 K. The spectrum of the flash-frozen solution reveals negative peaks at 1970 and 1981 cm^{-1} in addition to previously reported [13] negative bands at 1977 and 1985 cm^{-1} due to heme-bound CO and an asymmetric band near 2050 cm^{-1} due to photolyzed CO. The fractional contribution of the 1981 cm^{-1} band to the heme–CO absorbance envelope decreased from 25% to 15% after equilibrating the solution by scanning the cryostream temperature to 300 K and returning to 100 K over a period of ~1 h. Comparison of crystal and solution spectra reveals small changes in the frequencies and relative areas of the negative bands. These changes may indicate small conformational perturbations, but it is clear that the coordination of the heme and Cu sites is unaltered upon crystallization.

Detailed curve fitting analysis on the spectra reported in Fig. 3, as well as additional single crystal spectra (see Fig. S4), had the primary goal of quantifying spectral areas. For crystals that had not been exposed to X-rays, four Gaussian lines fit the negative heme–CO bands. Although only one peak was resolved for the positive-going 2050 cm^{-1} feature, two unresolved Gaussian lines were required to capture its asymmetry, suggesting the presence of unresolved contributions. We observe only slightly decreased C–O frequencies ($\leq$0.4 cm^{-1}) for the dominant bands when bound to the heme in

[3] The visible absorption spectrum of the single crystal reveals yet a fourth path to obtaining the crystal structure of electronically reduced cytochrome ba_3. Previous procedures were: (path A) treatment of the oxidized, as-isolated protein with a cryoprotectant solution containing excess dithionite followed by cryo freezing; (path B) by X-ray radiation of crystals held in a cryostream; (path C) by growth of crystals of the dithionite-reduced protein in an anaerobic environment prior to freezing in liquid nitrogen; and now (path D) treatment of crystals of as-isolated ba_3 that have been reduced with dithionite in the presence of CO followed by freezing. Notably, path D crystals do not show the unusual ~590 nm peak characteristic of those obtained by the A- and B-path, and to a lesser extent by the C-path (see Fig. S2).

ba_3–CO crystals, similar to early infrared measurements on polycrystalline samples of bovine cytochrome *c* oxidase, which found the dominant C–O frequency within 0.2 cm^{-1} of its value in solution [34]. However, the relative contribution of the 1977 cm^{-1} band increases at the expense of the 1981 and 1985 cm^{-1} bands in the crystal, contributing to a heme–CO frequency centroid 1 cm^{-1} lower than in solution (Table 3). A satisfactory fit still requires the 1981 cm^{-1} band, although it only contributes 9 ± 2% of the integrated heme–CO absorbance in the crystal. Any shift in the frequency of photolyzed CO is within our experimental uncertainty.

We could not count on observing dichroic absorption because of the high crystal symmetry, and no attempt was made to control the orientation of the crystal axes with respect to the IR beam. Nevertheless, the absorbance of oriented molecules in the crystal depends on the angle δ between the vibrational transition dipole and the tetragonal axis, and may be larger or smaller than the absorbance of randomly oriented molecules in solution [35]. As a result, there is no *a priori* reason to expect the molar absorbances of individual C–O bands to stand in the same ratio in single crystals and in solution.

Accordingly, significance is attached to the fact that the ratio of integrated C–O absorbance after photolysis to that before is similar, if not identical, to that observed in solution (Fig. 3, upper section). There is significant quantitative variation from crystal to crystal, reflected in the large standard deviation reported for this ratio in Table 3, which likely results from variations in the relative absorbance of individual bands for differently oriented crystals. In contrast, the ratio of positive and negative band areas is highly reproducible in photolysis and annealing measurements on the same crystal. The observation of similar ratios in crystals and solutions is consistent with measurable, but small, changes in CO orientation with respect to the tetragonal axis, upon photolysis.

We cannot exclude the possibility that similar orientation effects account for the slightly enhanced relative area of the 1977 cm^{-1} band in the crystal. However, variations in its relative area (40 ± 2% of the Fe–CO absorbance among the same group of crystals) are considerably smaller than those observed for the heme/Cu C–O band ratio. Dichroic IR absorption measurements on oriented crystals of lower symmetry would enable more quantitative structural conclusions about variations in CO orientation. While these are important details, overall, the FTIR observations confirm the notion that upon photolysis most, if not all, the CO bound to Fe_{a3} shifts to Cu_B where it clearly forms a coordinate covalent bond, most likely between the C-atom of CO and Cu_B. As noted by Woodruff and colleagues, this photolytic transfer of CO from Fe_{a3} to Cu_B occurs in <1 ps [36].

3.3. Evidence for radiation damage

Infrared measurements also show evidence of X-ray radiation damage. Specifically, after 18.4 MGy absorbed dose, the absolute IR spectra of crystals A3 (Fig. 2, lower section) and A2_2 (20.8 MGy, not shown) exhibited spectral features at 2133, 2165, 2255,and 2337 cm^{-1}, in addition to the 2050 cm^{-1} feature observed in crystals that had not been X-irradiated. Similar features have been observed to depend on radiation dose in butyrylcholinesterase crystals [35]. Decarboxylation of asparate or glutamate residues is a common radiation-induced modification [37] and the CO_2 produced would absorb near 2337 cm^{-1}, although the 2133 and 2337 cm^{-1} features also appear in irradiated mother liquor [35]. We previously reported CO_2 signals following blue or UV light-induced decarboxylation of Glu122 in green fluorescent protein (GFP) [38]. The decrease of the 2133, 2255, and 2337 cm^{-1} bands, observed upon annealing crystal

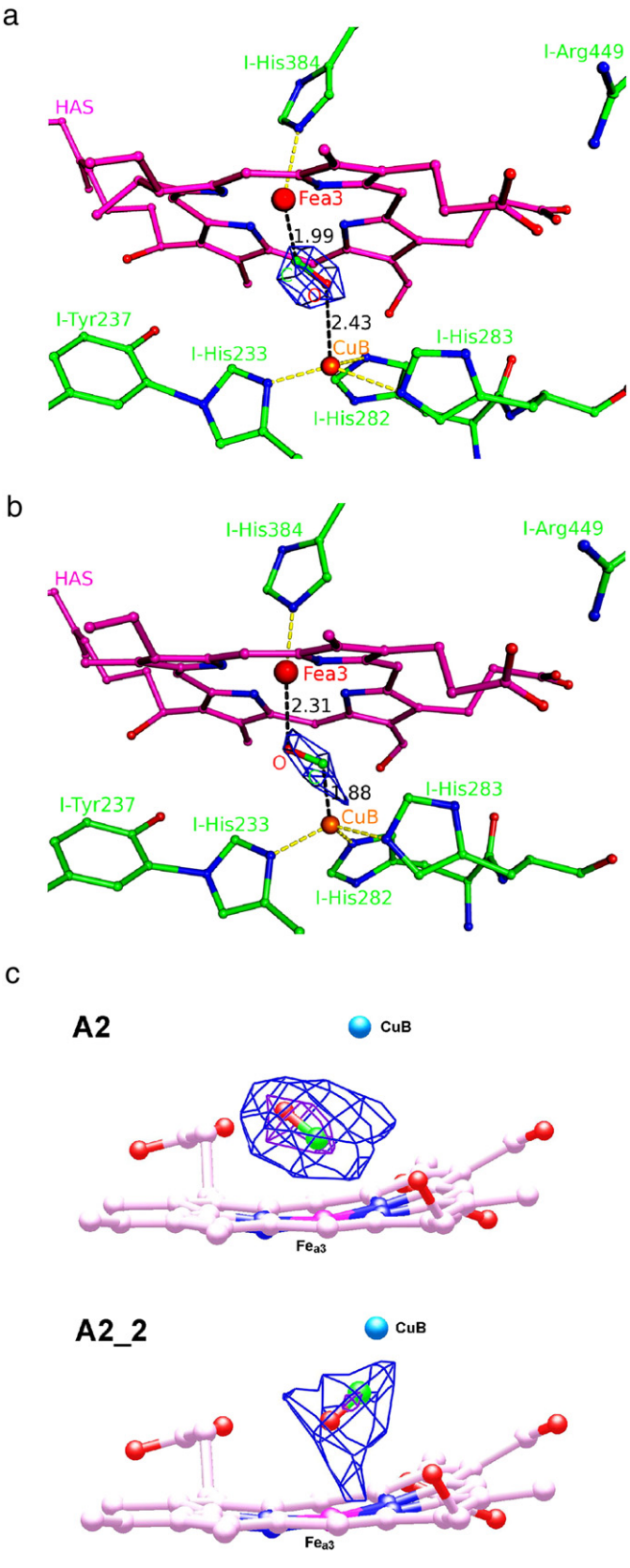

Fig. 1. Active sites of CO-bound reduced cytochrome ba_3 oxidase structure. The blue F_o–F_c maps are unbiased difference maps before including CO in the model. **(a)** A Fe–C–O bent binding mode to Fe_{a3} is indicated. The blue F_o–F_c map is contoured at 4σ for the A2 dataset. (**b**) Subsequent to performing photolysis of the same crystal during single crystal spectrophotometry (see Fig S2), the CO shifted to the Cu_B site. The blue F_o–F_c map is contoured at 3.5σ for the A2_2 data set. (**c**) Stick models showing orientation of Fe-bound and Cu-bound CO upon superposition of the structures of A2 (obtained before photolysis) and A2_2 (after photolysis and without annealing). The unbiased, sigma-weighted, F_o–F_c maps are contoured at 3σ (blue) and 4σ (inner, violet). Metrics are provided in (**a**) and (**b**).

Table 2
Bond lengths and bond angles at the active site.

[a]Data set	A2 Dark	A2_2 Light	J2 Dark	L1 Dark	C1 Light	E7 Light	Averages[b]
[c]Fe_{a3}–C (Å)	1.99		1.95	1.92			1.95 ± 0.04
[d]Fe_{a3}CO(°)	125.9		137.3	114.3			126 ± 8
[e]Cu_B–O (Å)	2.43		2.25	2.57			2.42 ± 0.11
[f]Cu_B–C (Å)		1.88			1.96	1.92	1.92 ± 0.03
[g]Cu_B–C–O (°)		112.12			132.1	144.46	129 ± 20
[h]Fe_{a3}–O (Å)		2.31			3.44	2.36	2.70 ± 0.49

[a] Data set for crystal designation to the right.
[b] Mean ± mean deviation.
[c] Fe to C-atom of the Fe bound CO in Å.
[d] Angle formed by Fe_{a3}, the C-atom of CO, and the O-atom of F_{ea3}-bound CO in degrees.
[e] Distance from Cu_B to the O-atom of the Fe_{a3}-bound CO in Å.
[f] Distance from Cu_B to the C-atom of the Cu_B-bound CO in Å.
[g] Angle formed from Cu_B to the C-atom and the O atom of the Cu_B-bound CO.
[h] Distance from Fe_{a3} to the O-atom of Cu_B-bound CO in Å.

A3 (Fig. 2, lower section), is consistent with outgassing of the corresponding molecular species at higher temperatures. In contrast with GFP, multiple components are not directly resolved in the 2337 cm^{-1} feature of irradiated ba_3 crystals, but a 2 cm^{-1} red shift upon annealing crystal A3, accompanied by a decrease in the FWHM from 10 to 7.5 cm^{-1}, suggests a distribution of CO_2 environments

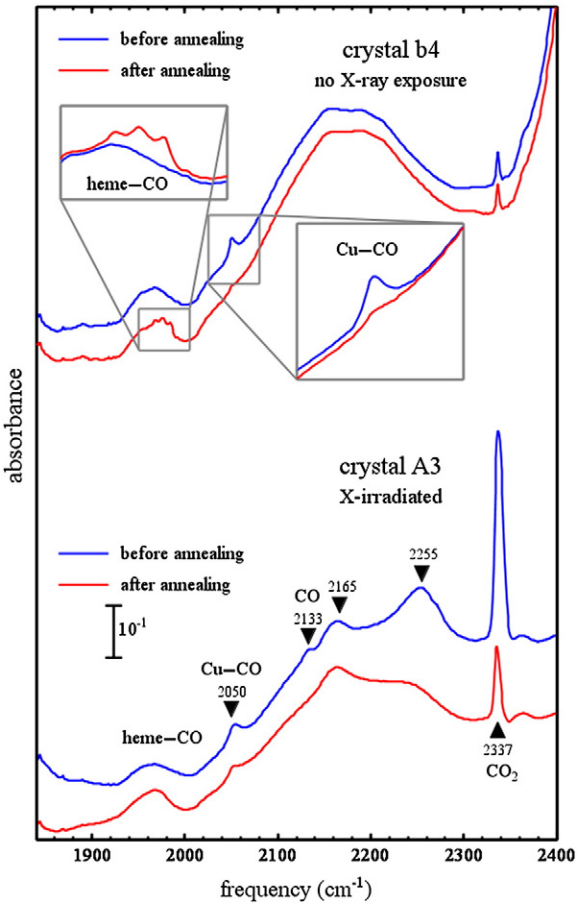

Fig. 2. Absolute infrared absorption spectra show changes that result from annealing any photolyzed ba_3–CO crystal that had not been exposed to X-ray irradiation (upper spectra). These include the loss of the 2050 cm^{-1} signal due to photolyzed CO and reappearance of heme–CO bands near 1980 cm^{-1}. Absolute spectra of crystal A3, irradiated with X-rays as described in Section 3.1 (bottom spectra), reveal additional bands at 2133, 2165, 2255, and 2337 cm^{-1}, in addition to the 2050 cm^{-1} Cu–CO band, reflecting molecular species that result from extended X-irradiation during collection of diffraction data. All but the 2165 cm^{-1} band decrease in intensity upon annealing.

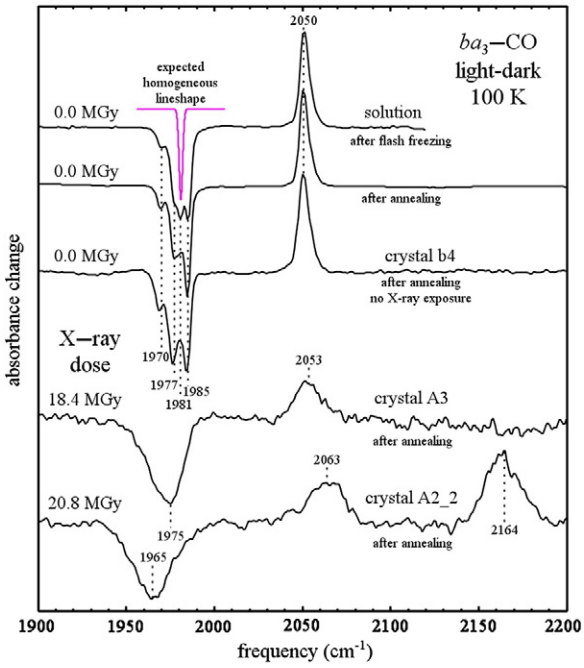

Fig. 3. Difference infrared absorbance changes in the C–O stretching region resulting from illumination of ba_3–CO with visible light probe the effects of crystallization and X-ray exposure on the structure of the catalytic site. Negative bands near 1980 cm^{-1} are due to CO bound to Fe_{a3} and an asymmetric positive band near 2050 cm^{-1} represents the photolyzed CO. The lineshape expected for an instrumentally broadened, homogeneous heme-bound C–O oscillator is indicated in magenta. Broadening of C–O bands in crystals exposed to the X-ray doses given for the two lower spectra is evident and reflects significantly increased structural disorder at the catalytic site. In contrast, the spectral features of unexposed crystals (middle spectrum) closely resemble those of solutions (two upper spectra). All results are differences between measurements recorded before and after photolysis with a microscope illuminator at 100 K.

that outgas at different rates. (A weak, narrower band observed in some unexposed crystals is consistent with the condensation of atmospheric CO_2 on the crystal surface during handling.) More detailed investigations will be needed to establish the molecular products responsible for these features and the associated protein structural modifications.

The feature near 2050 cm^{-1} decreases upon annealing, and the CO bands in the difference spectra resulting from subsequent photolysis of crystal A3 (Fig. 3, lower section) are significantly broadened and shifted in frequency relative to unexposed crystals (Fig. 3, Table 3). Similarly broadened CO absorption features were observed for crystal A2_2, and the 26 cm^{-1} linewidth obtained by fitting a Gaussian to the heme CO band indicate that the structural order of the active site decreases during the collection of X-ray diffraction data. The frequency shifts reflect changes in the *average* structure of the binuclear site as well, particularly for crystal A2_2. However,

Table 3
Spectroscopic properties of the stretching vibration of CO in the catalytic site of cytochrome ba_3.

	Dose (MGy)	Centroid frequency (cm^{-1})		Area ratio
		Heme–CO	Cu–CO	Cu/heme
Solution	0.0	1980.4	2051.6	0.61
Unexposed crystals[a]	0.0	1979.0 ± 0.4	2051.4 ± 0. 2	0.56 ± 0.14
Irradiated crystal A3	18.4	1970.9	2053. 4	0.36
Crystal A2_2	20.8	1965.4	2063.7	0.44

[a] Mean and standard deviation of independent photolysis measurements on five single crystals.

calculations predict the C–O frequency to shift by at least 20 cm^{-1} upon dissociation of protonation of imidazole ligands to either metal [39,40]. The observed frequency shifts thus suggest relatively modest perturbations of the average structure of the heme–Cu site, perhaps in response to a change of global protein conformation. Although the heme–Cu distance may be affected, the retention of photoinduced transfer of the CO between heme and Cu indicates that at least minimal functional integrity persists following irradiation.

3.4. Spectral lineshapes and environmental inflexibility

Alben's pioneering work on mitochondrial cytochrome *c* oxidase [12,14] revealed unusually narrow C–O stretching bands that appear to distinguish heme–copper oxidases from other heme proteins. Careful analysis reveals that ba_3–CO is no exception. The linewidths (FWHM) of Gaussians fitted to the heme–CO bands range from 3.0 to 6.0 cm^{-1} in five crystals that had not been exposed to X-rays. The linewidth of the most reliably characterized band at 1985 cm^{-1} ranges from 4.4 to 4.8 cm^{-1}. If the vibrational dephasing time of the C–O oscillator is assumed to be the same as that measured for CO bound to myoglobin at room temperature [41], this is very close to the 4.7 cm^{-1} homogeneous linewidth expected for a measurement at 2 cm^{-1} resolution. The longer dephasing time reported for Mb at 80 K [41] predicts a 2.4 cm^{-1} linewidth, as indicated by the magenta peak in Fig. 2. Each line therefore represents a highly ordered local environment.

In contrast, inhomogeneous broadening typically dominates the C–O linewidth in typical heme proteins. For example, 13 cm^{-1} C–O linewidths are observed for myoglobin, both in solution and in crystals [35,41]. The much narrower lines seen in heme–copper oxidases suggest a more ordered environment for the catalytic site. (As perspective on the discussion in the previous section, it is of interest to note that the intrinsic structural disorder of myoglobin appears intermediate between that observed for ba_3 before and after collection of diffraction data.) It is conceivable that this inflexibility serves a functional role. For example, structural rigidity could facilitate efficient proton transfer by preventing thermal disruption of Grotthuss-style proton "wires" (see Chang et al. [42]).

One exception to the narrow lines generally observed for heme–Cu oxidases is the 13 cm^{-1} C–O bandwidth reported for the cbb_3 heme–Cu oxidase from *P. stutzeri* at ambient temperature [43]. One of the histidine ligands in cbb_3 forms a cross-link with the Tyr from a neighboring helix, in contrast with more heavily investigated heme–Cu oxidases, where the cross-link forms with an adjacent Tyr side chain on the same helix. Minor β-conformations of heme–Cu oxidases have increased C–O linewidths, and also exhibit reduced catalytic activity [44]. Further work is needed to clarify the structural features responsible for narrow C–O linewidths in heme–Cu oxidases and their potential functional ramifications.

4. Summary and conclusions

In summary, the X-ray diffraction data support the idea that the photolyzed Fe_{a3}–CO complex of ba_3 is indeed a Cu_B–CO complex. The formation of this complex can be viewed as resulting from a rotation of ~180° around a normal to the C – O bond combined with a small translation away from the Fe toward the Cu, as shown in Fig. 1c. The nature of the chemical bonding within this atomic arrangement remains to be established. Finally, given that the "light"–"dark" FTIR difference spectrum of crystalline ba_3 is highly similar to that of detergent solubilized enzyme, it is certain that the dominant product of Fe_{a3}–CO photolysis within crystals and solutions is indeed Cu_B–CO, and that only small changes in metal coordination, outside the range of our resolution are likely to take place.

Acknowledgements

This study was supported by NIH grant GM35342 (JAF) and NSF grant CHE-1026369 (JTS). Part of this research was carried out at the Stanford Synchrotron Radiation Lightsource, a national user facility operated by Stanford University on behalf of the US Department of Energy, Office of Basic Energy Sciences. The SSRL Structural Molecular Biology Program is supported by the Department of Energy, Office of Biological and Environmental Research, and by the National Institutes of Health, National Center for Research Resources, Biomedical Technology Program, and the National Institute of General Medical Sciences.

Appendix A. Supplementary data

Supplementary data to this article can be found online at doi:10.1016/j.bbabio.2011.12.010.

References

[1] B.H. Zimmermann, C.I. Nitsche, J.A. Fee, F. Rusnak, E. Munck, Properties of a copper-containing cytochrome ba_3: a second terminal oxidase from the extreme thermophile *Thermus thermophilus*, Proc. Natl. Acad. Sci. U. S. A. 85 (1988) 5779–5783.
[2] J.A. Keightley, B.H. Zimmermann, M.W. Mather, P. Springer, A. Pastuszyn, D.M. Lawrence, J.A. Fee, Molecular genetic and protein chemical charactertization of the cytochrome ba_3 from *Thermus thermophilus* HB8, J. Biol. Chem. 270 (1995) 20345–20358.
[3] M.M. Pereira, M. Santana, M. Teixeira, A novel scenario for the evolution of haem–copper oxygen reductases, Biochim. Biophys. Acta 1505 (2001) 185–208.
[4] T. Yoshida, R.M. Lorence, M.G. Choc, G.E. Tarr, K.L. Findling, J.A. Fee, Respiratory proteins from the extremely thermophilic aerobic bacterium, *Thermus thermophilus*. Purification procedures for cytochromes c_{552}, $c_{555,549}$, and c_1aa_3 and chemical evidence for a single subunit cytochrome aa_3, J. Biol. Chem. 259 (1984) 112–123.
[5] T. Soulimane, G. Buse, G.B. Bourenkov, H.D. Bartunik, R. Huber, M.E. Than, Structure and mechanism of the aberrant ba_3-cytochrome *c* oxidase from *Thermus thermophilus*, EMBO J. 19 (2000) 1766–1776.
[6] L.M. Hunsicker-Wang, R.L. Pacoma, Y. Chen, J.A. Fee, C.D. Stout, A novel cryoprotection scheme for enhancing the diffraction of crystals of the recombinant, integral-membrane cytochrome ba_3 from *Thermus thermophilus*, Acta Crystallogr. D61 (2005) 340–343.
[7] T. Tiefenbrunn, W. Liu, Y. Chen, K. V., C.D. Stout, J.A. Fee, V. Cherezov, High resolution structure of the ba3 cytochrome *c* oxidase from *Thermus thermophilus* in a lipidic environment, PLoS One 6 (2011) e22348.
[8] J.A. Fee, D.A. Case, L. Noodleman, Toward a chemical mechanism of proton pumping by the B-type cytochrome *c* oxidases: application of density functional theory to cytochrome ba_3 of *Thermus thermophilus*, J. Am. Chem. Soc. 130 (2008) 15002–15021.
[9] S.A. Siletsky, I. Belevich, A. Jasaitis, A.A. Konstantinov, M. Wikström, T. Soulimane, M.I. Verkhovsky, Time-resolved single-turnover of ba_3 oxidase from *Thermus thermophilus*, Biochim. Biophys. Acta 1767 (2007) 1383–1392.
[10] I. Szundi, C. Funatogawa, J.A. Fee, T. Soulimane, O. Einarsdottir, CO impedes superfast O2 binding in ba3 cytochrome oxidase from Thermus thermophilus, Proc. Natl. Acad. Sci. U. S. A. 107 (2010) 21010–21015.
[11] X. Ye, A. Demidov, P.M. Champion, Measurements of the photodissociation quantum yields of MbNO and MbO_2 and the vibrational relaxation of the six-coordinate heme species, J. Am. Chem. Soc. 124 (2002) 5914–5924.
[12] J.O. Alben, P.P. Moh, F.G. Fiamingo, R.A. Altschuld, Cytochrome oxidase (a_3) heme and copper observed by low-temperature Fourier transform infrared spectroscopy of the CO complex, Proc. Natl. Acad. Sci. U. S. A. 78 (1981) 234–237.
[13] Ò. Einarsdóttir, P.M. Killough, J.A. Fee, W.H. Woodruff, An infrared study of the binding and photodissociation of carbon monoxide in cytochrome ba_3 from *Thermus thermophilus*, J. Biol. Chem. 264 (1989) 2405–2408.
[14] F.G. Fiamingo, R.A. Altschuld, P.P. Moh, J.O. Alben, Dynamic interactions of CO with a_3Fe and Cu_B in cytochrome *c* oxidase in beef heart mitochondria studied by Fourier transform infrared spectroscopy at low temperature, J. Biol. Chem. 257 (1982) 1639–1650.
[15] E. Pinakoulaki, U. Pfitzner, B. Ludwig, C. Varotsis, The role of the cross-link His-Tyr in the functional properties of the binuclear center in cytochrome *c* oxidase, J. Biol. Chem. 277 (2002) 13563–13568.
[16] G.T. Babcock, M. Wikström, Oxygen activation and the conservation of energy in cell respiration, Nature 356 (1992) 301–308.
[17] W.H. Woodruff, Coordination dynamics of heme–copper oxidases. The ligand shuttle and the control and coupling of electron transfer and proton translocation, J. Bioenerg. Biomembr. 25 (1993) 177–188.
[18] E. Pinakoulaki, Y. Yoshimura, V. Daskalakis, S. Yoshioka, S. Aono, C. Varotsis, Two ligand binding sites in the O_2-sensing signal transducer HemAT: implications for ligand recognition/discrimination and signalling, Proc. Natl. Acad. Sci. U. S. A. 103 (2006) 14796–14801.
[19] T.G. Spiro, I.H. Wasbotten, CO as a vibrational probe of heme protein active sites, J. Inorg. Biochem. 99 (2005) 24–44.

[20] L.Y. Fager, J.O. Alben, Structure of the carbon monoxide binding site of hemocyanins studied by Fourier transform infrared spectroscopy, Biochemistry 11 (1972) 4786–4792.
[21] Y. Chen, L.M. Hunsicker-Wang, R.L. Pacoma, E. Luna, J.A. Fee, A homologous expression system for obtaining engineered cytochrome ba_3 from *Thermus thermophilus* HB8, Protein Expr. Purif. 40 (2005) 299–318.
[22] B. Liu, V.M. Luna, Y. Chen, C.D. Stout, J.A. Fee, An unexpected outcome of surface engineering an integral membrane protein: improved crystallization of cytochrome ba_3 from *Thermus thermophilus*, Acta Crystallogr. F63 (2007) 1029–1034.
[23] A.G.W. Leslie, Joint CCP4 and ESF-EAMCB Newsletter on Protein Crystallography, 1992.
[24] S. Bailey, The CCP4 suite — programs for protein crystallography, Acta Crystallographica Section D-Biological Crystallography, 1994, pp. 760–763.
[25] R.J. Read, Pushing the boundaries of molecular replacement with maximum likelihood, Acta Crystallogr. D 57 (2001) 1373–1382.
[26] G.N. Murshudov, A.A. Vagin, E.J. Dodson, Refinement of macromolecular structures by the maximum-likelihood method, Acta Crystallogr. D 53 (1999) 240–255.
[27] P. Emsley, K. Cowtan, Coot: model-building tools for molecular graphics, Acta Crystallogr. D 60 (2004) 2126–2132.
[28] W.L. DeLano, The PyMOL Molecular Graphics System, DeLano Scientific, San Carlos, CA, 2002.
[29] K.S. Paithankaar, E.F. Garman, Know your dose: RADDOSE, Acta Crystallogr. D66 (2010) 381–388.
[30] B. Liu, Y. Chen, C.D. Stout, S.M. Soltis, T. Doukov, J.A. Fee, Combined microspectrophotometric and crystallographic examination of chemically-reduced and X-ray radiation reduced forms of cytochrome ba_3 from *Thermus thermophilus*: structure of the reduced form of the enzyme, Biochemistry 48 (2009) 820–826.
[31] Ò. Einarsdóttir, R.B. Dyer, P.M. Killough, F.J. A., W.H. Woodruff, Fourier transform infrared and resonance Raman characterization of cytochrome ba_3 from *Thermus thermophilus*, in: F. Adar, J.E. Griffiths, J.M. Lerner (Eds.), Proc. SPIE — The International Society for Optical Engineering, 1989, pp. 254–262.
[32] S. Yoshikawa, K. Shinzawa-Itoh, R. Nakashima, R. Yaono, E. Yamashita, N. Inoue, M. Yao, M.J. Fei, C.P. Libeu, T. Mizushima, H. Yamaguchi, T. Tomizaki, T. Tsukihara, Redox-coupled crystal structural changes in bovine heart cytochrome *c* oxidase, Science 280 (1998) 1723–1729.
[33] K. Muramoto, K. Ohta, K. Shinzawa-Itoh, K. Kanda, M. Taniguchi, H. Nabekura, E. Yamashita, T. Tsukihara, S. Yoshikawa, Bovine cytochrome c oxidase structures enable O_2 reduction with minimization of reactive oxygens and provide a proton-pumping gate, Proc. Natl. Acad. Sci. U. S. A. 107 (2010) 7740–7745.
[34] M. Tsubaki, K. Shinzawa, S. Yoshikawa, Effects of crystallization on the heme–carbon monoxide moiety of bovine heart cytochrome *c* oxidase carbonyl, Biophys. J. 63 (1992) 1564–1571.
[35] J.T. Sage, Y. Zhang, J. McGeehan, R.B.G. Ravelli, M. Weik, J.J. van Thor, Infrared protein crystallography, Biochim. Biophys. Acta 1814 (2011) 760–777.
[36] R.B. Dyer, K.A. Peterson, P.O. Stoutland, W.H. Woodruff, Ultrafast photoinduced ligand transfer in carbonmonoxy cytochrome c oxidase. Observation by picosecond infrared spectroscopy, J. Am. Chem. Soc. 113 (1991) 6276–6277.
[37] J.-P. Colletier, D. Bourgeois, B. Sanson, D. Fournier, J.L. Sussman, M. Weik, Shoot-and-trap: use of specific X-ray damage to study structural protein dynamics by temperature-controlled cryo-crystallography, Proc. Natl. Acad. Sci. U. S. A. 105 (2008) 11742–11747.
[38] J.J. van Thor, G.Y. Georgiev, M. Towrie, J.T. Sage, Ultrafast and low barrier motions in the photoreactions of the green fluorescent protein, J. Biol. Chem. 280 (2005) 33652–33659.
[39] S. Franzen, Effect of a charge relay on the vibrational frequencies of carbonmonoxy iron porphine adducts: the coupling of changes in axial ligand bond strength and porphine core size, J. Am. Chem. Soc. 123 (2001) 12578–12589.
[40] V. Daskalakis, E. Pinakoulaki, S. Stavrakis, C. Varotsis, Probing the environment of CuB in heme–copper oxidases, J. Phys. Chem. B111 (2007) 10502–10509.
[41] C. Rella, K.D. Rector, A. Kwok, J.R. Hill, H.A. Schwettman, D.D. Dlott, M.D. Fayer, Vibrational echo studies of myoglobin-CO, J. Phys. Chem. 100 (1996) 15620–15629.
[42] H.-Y. Chang, J. Hemp, Y. Chen, J.A. Fee, R.B. Gennis, The cytochrome ba3 oxygen reductase from *Thermus thermophilus* uses a single input channel for proton delivery to the active site and for proton pumping, Proc. Natl. Acad. Sci. U. S. A. 1090 (2009) 16169–16173.
[43] S. Stavrakis, K. Koutsoupakis, E. Pinakoulaki, A. Urbani, M. Saraste, C. Varotsis, Decay of the transient Cu_B–CO complex is accompanied by formation of the heme Fe–CO complex of cytochrome cbb_3–CO at ambient temperature: evidence from time-resolved Fourier transform infrared spectroscopy, J. Am. Chem. Soc. 124 (2002) 3814–3815.
[44] H. Ji, T.K. Das, A. Puustinen, M. Wikström, S.-R. Yeh, D.L. Rousseau, Modulation of the active site conformation by site-directed mutagenesis in cytochrome *c* oxidase from *Paracoccus denitrificans*, J. Inorg. Biochem. 104 (2010) 318–323.